УДК 535.4

MODE DECOMPOSITION METHOD FOR INVESTIGATING THE NONLINEAR DYNAMICS OF A MULTIMODE BEAM

© **M. Gervaziev[1,2], M. Ferraro[3], E. V. Podivilov[1,2], F. Mangini[3], O. S. Sidelnikov[2], D. S. Kharenko[1,2], M. Zitelli[3], M. P. Fedoruk[2], S. A. Babin[1,2], and S. Wabnitz[2,3]**

[1] *Institute of Automation and Electrometry SB RAS, 1 Ac. Koptyug ave., Novosibirsk, Russia*
[2] *Novosibirsk State University, 1 Pirogova str., Novosibirsk, Russia*
[3] *Department of Information Engineering, Electronics, and Telecommunications, Sapienza University of Rome, 00184 Rome, Italy, Via Eudossiana 18*
E-mail: gervaziev.m@gmail.com

We overview our recent experimental studies on the nonlinear spatial reshaping of multimode beams at the output of multimode optical fibers. We use a holographic mode decomposition technique, which permits to reveal the variation of the spatial mode composition at the fiber output, as determined by either conservative (the Kerr effect) or dissipative (Raman scattering) nonlinear processes. For the first case, we consider the effect of spatial beam self-cleaning, and we compare experimental mode decompositions with predictions based on the thermodynamic theory, including the case of beams carrying nozero orbital angular momentum. For the second case, we analyze the beam mode content at the output of a Raman laser based on a graded index multimode fiber.

Keywords: Mode decomposition, thermalization, multimode fiber.

DOI: 10.15372/AUT20230106

1. Introduction. Nonlinear optical effects are particularly effective in optical fibers, in spite of their relatively low nonlinearity. This is because of their small effective area and long guiding lengths, whose combination favor the observation of nonlinear phenomena such as the Kerr effect, Raman scattering, self-steepening, temporal soliton and supercontinuum generation [1–3]. Over the past decades, the large majority of research works focused on single-mode fibers. The propagation of a single mode naturally guarantees a high quality beam profile at the fiber output, which is relevant in many applications. Moreover, modal dispersion is absent in single-mode fibers, which rapidly made them the solution of choice for optical telecommunication links. Nevertheless, in recent years there has been a resurgence of interest in the use of multimode (MM) fibers. As their name conceptualizes, MM fibers permit the simultaneous propagation of a many guided modes, thanks to their larger core size with respect to single-mode fibers. Moreover, owing to their larger core area, MM fibers support the propagation of higher energy pulses with respect to single-mode fibers. These properties may permit, on the one hand, to overcome the current capacity crunch in single-mode fiber-based links, and, on the other hand, to scale up the energy of pulses (or the continuous-wave power) delivered by fiber lasers.

In MM fibers, guided modes may exchange their energy via either linear or nonlinear processes during their propagation. Indeed, the degree of freedom given by the mode interactions unravels a host of nonlinear phenomena, which are peculiar to MM fibers [4]. As discussed in recent works, multimodality synergetically merges with typical effects of nonlinear fiber

optics [5, 6], which are especially attractive for many applications of MM fibers, e.g., in medical and biological imaging. Another remarkable example is provided by the generation of spatiotemporal or MM solitons: originally theoretically predicted by Hasegawa in 1980 [7], these solitons not been experimentally characterized until quite recently [8, 9]. In addition, it is worth mentioning the work of [10], where the effect of soliton self-mode conversion was experimentally demonstrated. Exploiting fiber multimodality makes it possible to control the group velocity of nonlinear waves [10], to obtain phase-matching with parametric four-wave interactions [11], and to demonstrate the spatiotemporal mode locking of MM fiber lasers [12, 13].

Among the many novel phenomena, potentially relevant for applications is the so-called spatial beam-self cleaning (BSC) effect. BSC consists of the transformation, from speckles to a bell-shape, of the beam profile at the output of a MM fiber: this entails a substantial increase of the spatial beam quality or brightness [14]. As a matter of fact, the main disadvantage of MM fibers is the low spatial quality of radiation at their output. This is because the coherent superposition of a large number of modes with dfifferent relative phases leads to a highly speckled intensity profile [15]. In contrast, BSC permits to overcome this issue, which promises to widen the use of MM fibers in high-power photonic devices and systems.

Since its first observation in 2016 [11], it appeared evident that BSC is driven by the Kerr effect via degenerate four-wave-mixing processes. At a first sight one may think of BSC as a sort of beam condensation, where all of the beam power is transfered towards the fundamental MM fiber mode. However, it has been demonstrated that the occupancy of higher-order modes is not negligible in typical self-clened beams [16].

To date, a comprehensive understanding of the physical mechanisms which lay behind BSC is still under debate. Indeed, BSC has been described in analogy with 2D hydrodynamic turbulent systems, where most of the beam energy flows into the fundamental mode, with a concomitant redistribution of energy towards high-order modes [17]. A different description has also emerged, in the frame of a thermodynamic approach [18], where the fiber modes are seen as analogues to particles of a gas. It is worth to mention that four-wave-mixing is particularly effective in graded-index (GRIN) MM fibers, whose parabolic index profile enhances the four-wave interactions among many phase-matched spatial modes [19]. Indeed, so far virtually all the experimental observations of BSC in MM fibers are limited to the case of GRIN fibers.

In this regard, it must be noted that spatially cleaned beams may also be generated by exploiting Raman nonlinearity of MM fibers. In recent literature, several studies have reported how Stokes waves which are generated from MM pumps appear as bell-shaped beams [9, 20, 21]. This Raman clean-up effect unlocked the possibility of developing a new class of MM fiber lasers, which are referred to as Raman fiber laser (RFL).

Regardless of the type of nonlinearity involved in determining the nonlinear beam dynamics, the interactions among the multiple modes of MM fibers play a crucial role in determining the nonlinear beam evolution. This makes it necessary to develop appropriate mode decomposition (MD) techniques, which were missing in the 1980s, when theoretical studies of nonlinear beam dynamics in MM fibers were firstly reported [22, 23]. Indeed, various MD methods have been described in recent literature: these can be generally categorized in three groups, depending on whether they are based on deep learning and genetic algorithms [24, 25], complete wavefront characterization with a lateral shearing interferometer together with simple projection of the measured field on the modes [26, 27], or phase modulation and optical correlation filters [28, 29].

In this work we exploit a holographic MD technique, which belong to the last group, and used it for retrieving the power dependence of the mode content of laser beams at the output of GRIN MM fibers. At variance with other methods, which either permit to analyze a small number of modes, or provide a low resolution of the beam profile image, our method relies on high-resolution cameras, and it allows for determining both the amplitude and the phase

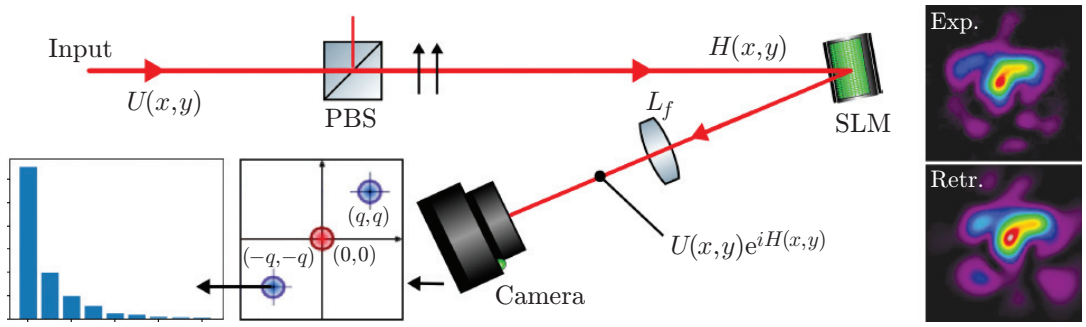

Fig. 1. Sketch of the experimental MD setup. The near-field at the output of a GRIN MM fiber $U(x, y)$ is projected onto the SLM, which encodes a phase $H(x, y)$. The polarization of the beam is filtered by means of the PBS. The lens L_f projects the Fourier transform of the modulated field onto a CCD camera which captures the first diffraction maximum (q,q), containing information about the amplitude or phase of each mode, and permitting to retrieve the mode occupancy distribution (histogram in the bottom left corner). An example of measured and reconstructed distributions is shown on the right side of the figure

associated with a relatively large number (up the order of a hundred) of guided modes. We apply this holographic MD method to the analysis of BSC beams, and to the study of the nonlinear evolution of orbital angular momentum (OAM) beams. Moreover, we also consider beam propagation driven by the Raman nonlinearity. Specifically, we analyze the mode content at the output of a RFL system. This work is organized as follows. In Section 2, we describe the holographic MD method; in Section 3, we exploit this method for confirming theoretical previsions of the statistical mechanics approach to nonlinear beam dynamics; in particular, we experimentally verify that the phenomenon of BSC can indeed be described within a statistical mechanics framework;in Section 4 we applied the holographic MD method to a RFL system. Finally, in Section 5, we draw the conclusions.

2. Holographic mode decomposition. The holographic MD technique is implemented by using a spatial light modulator (SLM), which is a computer-controlled device that imposes some form of spatial modulation (amplitude, phase, or amplitude-phase) on radiation. In particular, here we rely on a phase-only SLM, which encodes a phase $H(x, y)$ to the near-field of the beam to be decomposed $U(x, y)$ (see the sketch in Fig. 1). Being at the output of a GRIN MM fiber, the latter can be represented as a superposition of Laguerre-Gaussian (LG) [30–32] modes, which are the eigenmodes of this fiber. Formally, this can be represented as:

$$U(x,y) = \sum_{\text{even,odd}} \sum_{m,p=0}^{\infty} B_{mp} \cdot \psi_{mp}(x,y), \tag{1}$$

where B_{mp} is the complex amplitude of modes with principal quantum number $n = 2p + |m|$, m is the orbital quantum number and p is the radial quantum number.

The main objective of MD consists of determining the values of B_{mp}. Mathematically, this can be expressed as a simple dot product: $B_{mp} = \langle \psi_{mp} \mid U \rangle$. In practice, such an operation can be implemented by using a spatial filter with a transmission function $T_{mp}(x, y)$ equal to $\psi^*_{mp}(x, y)$, and a Fourier lens (L_f in Fig. 1) acting as an integrator [33]. In order to determine the contribution of each mode, different phase patterns are reproduced on the SLM, which transform the SLM transmission function into $T_{mp}(x, y)$ up to certain coefficient. In the Fourier

plane, the intensity distribution I_{mp} is measured by means of the camera depicted in Fig. 1, which can be expressed as:

$$I_{mp}(x', y') = |B'_{mp}(x', y')|^2 = \Big| \int\limits_{-\infty}^{\infty} T_{mp}(x, y) U(\vec{\rho}(x, y)) \, \mathrm{e}^{i(xx'+yy')} \, dx \, dy \Big|^2. \tag{2}$$

Hence $B'_{mp}(x', y')|_{(0,0)} = B_{mp}$, that is, the field amplitude at the center of the Fourier plane, gives the exact desired value of the mode amplitude. In order to check the correctness of the results, it is necessary to recompose the beam and compare it with the original near-field profile. In order to do so, it is necessary to determine the intermodal phases. This can be done in the same way as with the amplitudes, by calculating the intermodal interference of each mode with the fundamental one, as described in [34].

Numerical simulations demonstrated the influence of various factors on the decomposition accuracy [35]; the most critical were the value of the spatial frequency shift (which must be a multiple of the sampling frequency), and the choice of the correlation answer point of intensity measurement (which must strictly correspond to the center of the correlation answer). The same work demonstrates methods for minimizing the negative impact of these factors, and reports a successful modal analysis of speckled beams propagating in a GRIN MM fiber containing ∼80 modes. Thus, it can be concluded that the SLM-based correlation filter method is suitable for accurately analyzing the modal content of radiation at the output of a MM fiber.

In our experiments, we used a 2 m long GRIN MM fiber with a core size of 50 μm and whose output facet was imaged onto the SLM by means of two confocal lenses (not shown in Fig. 1). Finally, we inserted a polarizing beam slitter (PBS in Fig. 1), in order to project the beam polarization vector on a given direction. As a matter of fact, the SLM only works for linearly polarized waves. Moreover, the experimental analysis was limited to the first 78 modes, i.e., only modes with $n \leq 11$ were considered. This number was chosen as a trade-off between a reasonable running time of the algorithm, and sufficiently high quality of the beam reconstruction.

3. Verification of optical beam thermalization. As a testbed for our MD tool, we consider a test of the validity of the beam thermalization theory for describing BSC in MM fibers. The thermodynamic approach has been first introduced by Aschieri et al. in 2011 [36], and recently expanded for framing the physics of highly multimode nonlinear optical systems within a thermodynamic description [18]. The thermodynamic relies on the the hypothesis that MM systems reach an equilibrium as a consequence of their nonlinear evolution, upon which some key physical parameters are conserved. For instance, when applied to MM fibers, one may consider the conservation of the total optical power (P), provided that there are no optical losses, of the Hamiltonian or total linear momentum (H), and of the total OAM (M), which is ensured by the cylindrical geometry of optical fibers.

According to the theory, at thermal equilibrium the modes approach a generalized Rayleigh-Jeans (R-J) distribution, which can be expressed in the ψ_{mp} base as [37]:

$$|B_{m,p}|^2 = \frac{1}{\alpha + \beta(2p + |m|) + \gamma m}. \tag{3}$$

where α, β, and γ are parameters which come from the conservation laws of P, H, and M, respectively. It is straightforward to demonstrate that

$$P \propto \sum_{m,p} |B_{m,p}|^2, \tag{4}$$

$$H \propto \langle n \rangle = \sum_{m,p} n \cdot |B_{m,p}|^2, \tag{5}$$

$$M \propto \langle m \rangle = \sum_{m,p} m \cdot |B_{m,p}|^2. \tag{6}$$

Owing to these proportionality relationships, it is possible to demonstrate the conservation of H and M by experimentally verifying the conservation of $\langle n \rangle$ and $\langle m \rangle$, respectively. In this regard, we underline that since the values of the intensity profiles recorded by the cameras are given in arbitrary units, the setup only makes it possible to estimate the relative values of the mode intensities, i.e., the value of the power fraction normalized to the total beam power. Finally, in order to ensure the conservation of P, we used a laser source emitting picosecond pulses at 1030 nm of wavelength (λ). Indeed, it is well known that at this wavelength the linear absorption is less than 1 dB/km [1]. Moreover, the thermodynamic theory only holds for weak nonlinearity, i.e., with peak powers of the order of a few kiloWatts, which are about three orders of magnitude lower than the values needed for triggering catastrophic self-focusing, as well as nonlinear absorption effects in standard MM fibers [38].

3.1. The spatial beam self-cleaning effect. Let us consider first the simplest case where the beam does not carry any OAM, i.e., $M = 0$. By combining eqs. (3) and (6), it is easy to demonstrate that $\gamma = 0$. Therefore, the equilibrium distribution (3) boils down to the standard R-J distribution, which no longer depends on the sign of m. In particular, the equilibrium distribution only depends on n. This result is given by a peculiarity of GRIN MM fibers, i.e., the equal spacing of its mode propagation constants [39].

Whenever $M = 0$, the thermodynamic theory applies to the description of the BSC effect [40–42]. Indeed, it can be seen in Fig. 2a how the occurrence of BSC is associated with an experimental mode distribution (histogram) that matches well with the theoretical R-J distribution (red line). To the contrary, when the laser input peak power (P_p) is too low for obtaining the BSC effect, the output beam has a speckled intensity profile: the corresponding mode distribution does not obey the R-J law (cfr. Fig. 2b). Indeed, the discrepancy between the experimental mode distribution and the R-J law is expected to be reduced, when moving from a speckled pattern (out-of-equilibrium beam) to a bell-shaped intensity profile (thermalized beam), i.e., by increasing P_p. This is shown in Fig. 2c, where we plot the root-mean-square error (RMSE) of the theoretical curve (eq. (3) with $\gamma = 0$), with respect to the experimental MD data. As it can be seen, despite some small fluctuations, the RMSE progressively quenches as P_p grows larger.

Finally, Fig. 2d shows that both H and M remain constant, within the experimental error, for all values of P_p. In particular, in agreement with theory, we found that $\langle m \rangle = 0$ (see the red dashed line in Fig. 2d). Moreover, modes having opposite sign of m turn out to have nearly the same occupancy (not shown), in agreement with the symmetry with respect to $m = 0$ of eq. (3) when $\gamma = 0$.

3.2. Thermalization of OAM-carrying beams. Let us now consider the general case with $M \neq 0$. Experimentally, this corresponds to injecting an OAM-carrying beam at the input of the MM fiber. This can be easily achieved in optical fibers by exploiting their cylindrical geometry. Indeed, in order to provide OAM to a Gaussian laser beam it is sufficient to inject it into the fiber core with nonzero tilt angle (ϑ) and transverse displacement (y_0) with respect to the fiber axis [43, 44]. In this way, the beam acquires an OAM, so that

$$\langle m \rangle_{\text{the}} = 2\pi \frac{y_0 \sin \vartheta}{\lambda}. \tag{7}$$

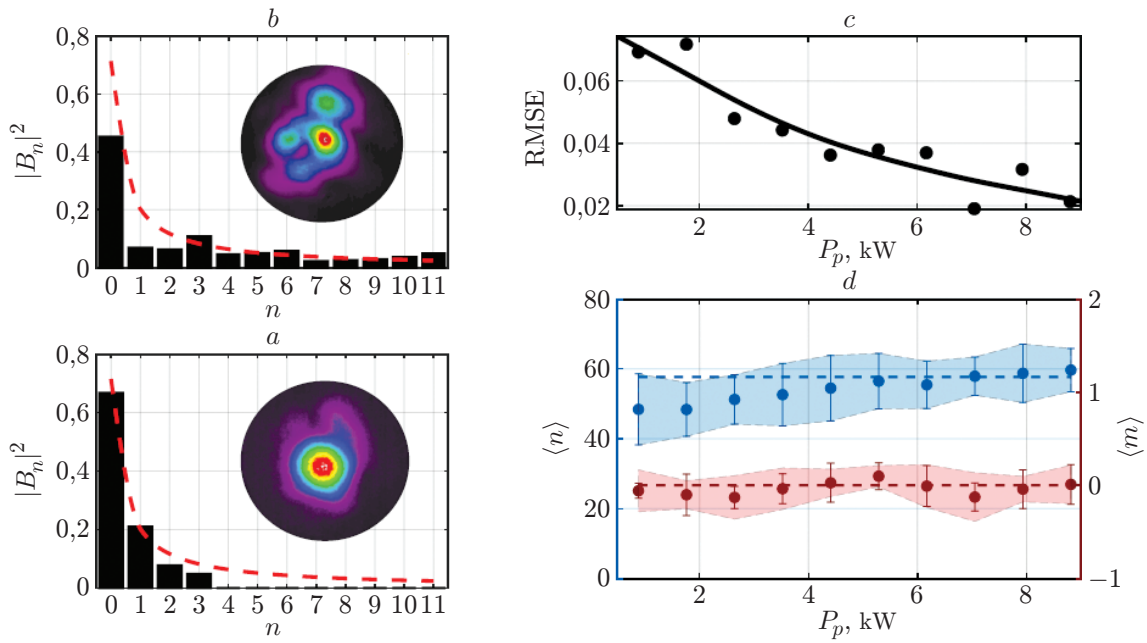

Fig. 2. a) Experimental MD (histogram) of a thermalized beam at $P_p = 8.81$ kW, i.e., at the occurrence of BSC. b) Experimental MD (histogram) of an out-of-equilibrium beam at $P_p = 0.88$ kW, i.e., at a power below the BSC threshold. The insets of (a) and (b) show the measured near-field intensity at the MM fiber output facet, whereas the dashed red line which is reported in both (a) and (b) is the fitting R-J law of the experimental data in (a). c) Root-mean-square-error between the experimental mode composition and the R-J law (3) as a function of P_p. (d) Values of $\langle n \rangle$ and $\langle m \rangle$ calculated from the experimental MD data as a function of P_p

The experimental results of the MD analysis are reported in Fig. 3. In particular, in Fig. 3a, we report how the RMSE between the experimental data and the theoretical prediction of eq. (3) is progressively reduced as the peak pulse power grows larger. In other words, similarly to the case of BSC, the RMSE quenches as P_p grows larger. This indicates that, whenever sufficient power is provided, the four-wave mixing processes allow for reaching beam thermalization, which, indeed, turns out to be well described by the generalized R-J law (3). Moreover, in analogy with the results in Section 3.1, we verified the validity of the hypothesis at the basis of the thermodynamic theory, i.e., the conservation laws of H and M. This is shown in Fig. 3b where we plot, as a function of P_p, the values of $\langle n \rangle$ and $\langle m \rangle$. These were computed from the values of $B_{m,p}$ provided by the holographic MD. As it can be seen, both $\langle n \rangle$ and $\langle m \rangle$ remain constant, within the experimental error. In particular, at variance with BSC, here we found that $\langle m \rangle \neq 0$.

The conservation of $\langle n \rangle$ and $\langle m \rangle$, which is associated with the conservation of linear and angular momentum, respectively, has been experimentally verified. As it can be seen, when P_p varies, both $\langle n \rangle$ and $\langle m \rangle$ fluctuate within experimental errors around the constant value of -0.25. Such a value is rather close to -0.21, which is the value predicted by eq. (7) when substituting the experimental parameters $\vartheta = 2°$ and $y_0 = -1$ μm.

4. Beam mode content at the output of a MM Raman fiber laser. Similar to the case of four-wave-mixing, also Raman scattering may be responsible for an increase of the spatial quality of laser beams. Indeed, it was recently shown that RFLs pumped by MM

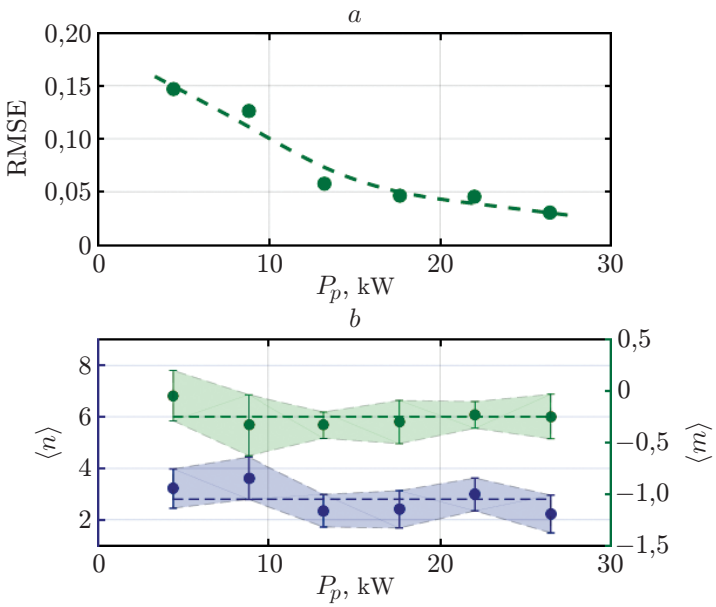

Fig. 3. a,b) Same as Fig. 2c,d when coupling the laser beam into the GRIN MM fiber within a tilt angle $\vartheta = 2°$ and an offset $y_0 = -1$ μm with respect to the fiber axis

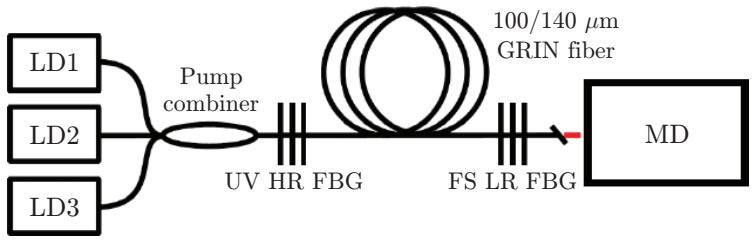

Fig. 4. Schematic of the RFL (LD: MM pumping laser diodes; UV HR FBG: strong-reflective FBG recorded by UV radiation; FS LR FBG: weak-reflective FBG recorded by femtosecond pulses)

laser diodes (LD) provide an efficient conversion mechanism for highly MM pump beams into Stokes beams with high quality [45–47]. In particular, in [48], the record level of brightness enhancement (BE = 73) was demonstrated, along with a value of M^2 equal to 2 with a power ∼50 W. As the low value of M^2 indicates, the Stokes beam has a nearly Gaussian shaped profile. Still, in analogy with BSC, the occupancy of higher-order modes is non negligible. Therefore, performing a MD analysis is crucial for investigating the physical processes that provide the complex nonlinear modal interactions that occur in a RFL.

Our MD tool was adapted to analyze the modal content of both the pump and the signal (Stokes) beams at the output of a continuous-wave (CW) RFL based on a GRIN fiber. In particular, a bandpass filter was added, in order to separately analyze the pump and the Stokes beams. A full description of the setup can be found in [49]. In Fig. 4 we limit ourselves to sketch the laser cavity, which was made with a piece of GRIN MM fiber with a core diameter of 100 μm, and with fiber Bragg gratings which acted as cavity mirrors. We underline that the generated Stokes radiation was previously investigated in terms of the beam quality parameter M^2 in [47] and beam profile in [48, 50]. An important detail of the laser is that the output fiber Bragg grating has a mode-selective reflection coefficient, since it was inscribed by means

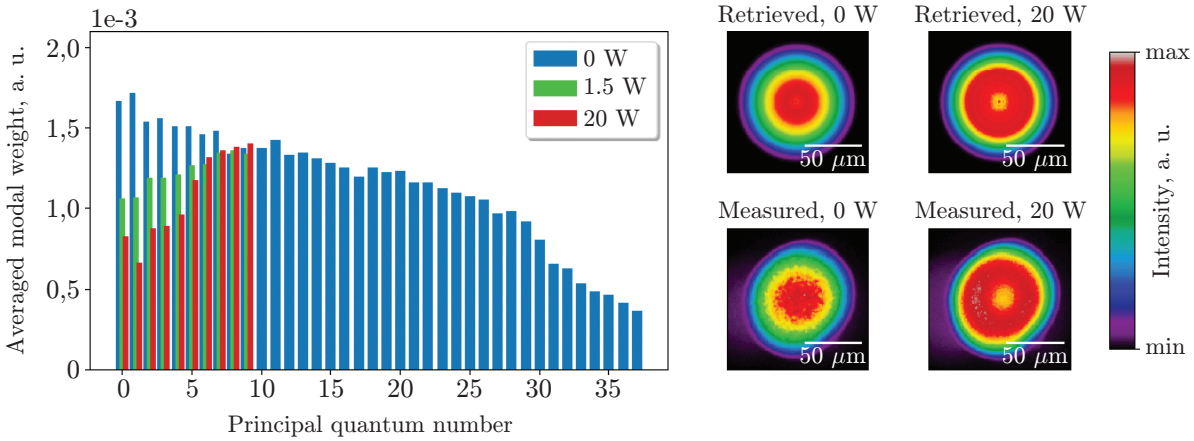

Fig. 5. Power distribution (histogram) of modes contributing to the pump beam, for different power values of the Stokes beam (indicated in the legend). The Raman threshold power is below 1.5 W. The modes are sorted by n and averaged by their degree of degeneracy; The images on the right are the reconstructed (retrieved) and measured profiles of the residual pump beam, respectively, under and well-above the lasing threshold

of a femtosecond laser in the central part of the fiber core. In this way, the fundamental mode reflection coefficient is 10 dB higher than that of higher-order modes. As a result, the generated Stokes beam is of high quality and has a narrow spectrum, with a single bell-shaped intensity peak determined by the predominant content of the fundamental mode [47, 48, 50].

As mentioned above, when analysing nonlinear beam dynamics dominated by the Kerr effect, we truncated our MD analysis to 78 modes. However, such a value is quite a small number for the full characterization of the pump beam of our RFL. As a matter of fact, according to previous studies [48, 50], radiation almost occupies the entire core of the GRIN fiber. Therefore, in this study the number of modes considered for MD was increased up to ∼780. In order to reduce the experiment time, which scales with the number of modes considered, we excluded measurements of the relative intermodal phase, which does not contribute to the resulting intensity distribution at the output, owing to the presence of a large number of longitudinal modes with random non-stationary phases. These steps allowed us to perform an accurate MD of Stokes radiation up to ∼20 W, as well as a MD of pump radiation.

The most interesting observation is the behavior of the mode distribution for the pump beam at $n < 10$, either below or above the Raman threshold. Indeed, we observed that above the Raman threshold the contribution of the first three LG modes ($LG_{0,0}$, $LG_{1,0}$, $LG_{-1,0}$), i.e., modes having $n \leq 1$, decreases by about 30% when the power grows larger (Fig. 5). It is clear that the first 5–7 principal quantum numbers (PQNs) are involved in the depletion process, which indicates the presence of significant interactions between the pump modes with different quantum numbers and the Stokes beam [49].

Our analysis of the Stokes radiation demonstrates that the fraction of the fundamental mode is about 40%, and more than 60% of all of the beam energy is concentrated in the first three modes only (Fig. 6). This leads to an increase in the brightness of the Stokes beam, when compared to the pump beam. At the same time, the data obtained show that the value of the previously measured parameter M^2 higher than 1 is associated with a significant contribution of $LG_{1,0}$ and $LG_{-1,0}$ modes to the output beam of the Stokes wave.

The distribution of modes in a dissipative system with coupled modes, such as the RFL, of course differs from the distribution observed in the case of a conservative system, such as

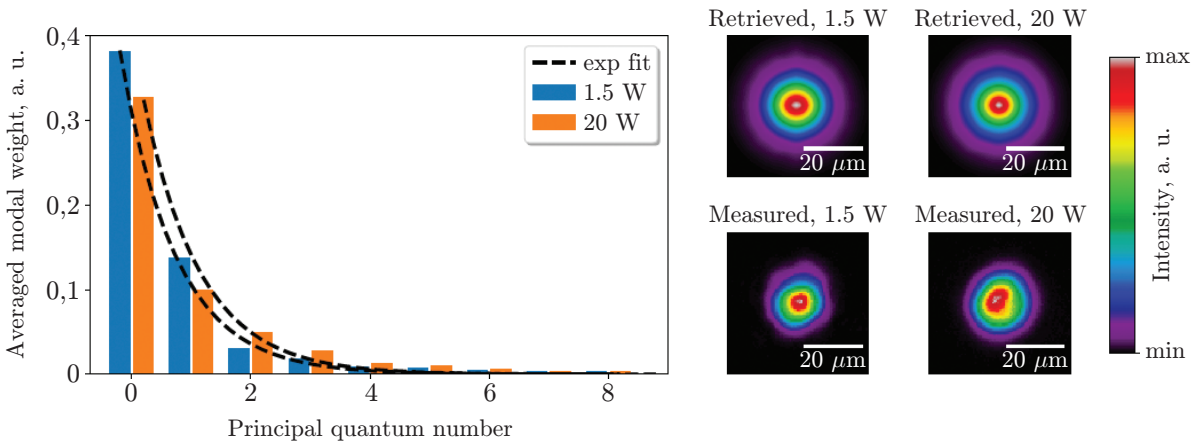

Fig. 6. Power distribution by modes contributing to the Stokes beam at low (1.5 W) and high (20 W) output power of the Stokes radiation component, sorted by PQN and averaged by degree of degeneracy of modes (left); reconstructed and measured output profiles of the Stokes beam (right). The dashed lines represent exponential fit curves

that dominated by Kerr nonlinearity. In this system, FBG gain and loss were present for each subsequent bypass of the cavity, so the distribution of modes is derived from a system of balance equations for mode powers. Several requirements apply in this system of equations: 1) the gain of the fundamental mode is much greater than the gain values for the other modes; 2) random linear coupling dominates over nonlinear effects; 3) linear coupling is highest for neighboring modes, while other coupling coefficients can be neglected. The final mode distribution can be described by the following exponential function:

$$P_k \simeq P_0 \, \mathrm{e}^{-k \ln (1/C^2)} \, . \tag{8}$$

where P_k is the power of the kth mode, C is a linear mode coupling coefficient.

When comparing the experimental distribution of modes with various analytical expressions, we can see that experiments are better described by the exponential distribution (shown by dashed lines in Fig. 6). This means that in a dissipative system with coupled modes one can observe a specific distribution, which is mainly determined by the special filtering properties of the modes with gain and loss, and the random characteristics of linear mode coupling.

5. Conclusions. In this work, we applied a MD technique based on digital holography in order to analyze the modal content of radiation propagating in nonlinear GRIN MM fibers. Specifically, we reported two study cases. In the first case, the nonlinear beam dynamics is dominated by degenerate four-wave-mixing processes. Whereas, the second study case was focused on a MM RFL. According to theoretical approaches based on statistical mechanics, at high input powers four-wave-mixing leads to an equilibrium distribution, which follows the R-J law. This has been experimentally verified, both in the presence and in the absence of OAM of light. In particular, in the former case, our results confirmed that the phenomenon of BSC can be described in terms of classical wave thermalization. A "clean"spatial profile was also observed for the Stokes wave generated by Raman scattering in a MM RFL. However, as we experimentally demonstrated, in such a MM system the mode distribution which is associated to a bell-shaped beam does not follow the R-J law. To the contrary, we proposed an empirical exponential law, which turns out to be in good agreement with experimental data.

Acknowledgements. We acknowledge the support of the European Research Council (740355), the Italian Ministry of Education and Research (R18SPB8227), Sapienza University (RG12117A84DA7437), and the Russian Science Foundation (21-42-00019).

REFERENCES

1. **G. P. Agrawal**, Nonlinear Fiber Optics /In Nonlinear Science at the Dawn of the 21st Century, p. 195–211. Springer, 2000.
2. **V. R. Supradeepa, Yan Feng, and J. W. Nicholson**, Raman fiber lasers. J. Opt., 19(2):23001, 2017.
3. **J. M. Dudley, Goëry Genty, and Stéphane Coen**, Supercontinuum generation in photonic crystal fiber. Rev. Mod. Phys., 78(4):1135–1184, oct 2006.
4. **I. Cristiani, C. Lacava, G. Rademacher, et al**, Roadmap on multimode photonics. J. Opt., 24(8):083001, aug 2022.
5. **A. Picozzi, G. Millot, and S. Wabnitz**, Nonlinear virtues of multimode fibre. Nature Photonics, 9(5):289–291, 2015.
6. **K. Krupa, A. Tonello, A. Barthélémy, et al.**, Multimode nonlinear fiber optics, a spatiotemporal avenue. APL Photonics, 4(11):110901, 2019.
7. **A. Hasegawa**, Self-confinement of multimode optical pulse in a glass fiber. Optics Letters, 5(10):416–417, 1980.
8. **W. H. Renninger and F. W. Wise**, Optical solitons in graded-index multimode fibres. Nature Communications, 4(1):1–6, 2013.
9. **M. Zitelli, F. Mangini, M. Ferraro, O. Sidelnikov, and S. Wabnitz**, Conditions for walk-off soliton generation in a multimode fiber. Communications Physics, 4(1):1–6, 2021.
10. **L. Rishøj, B. Tai, P. Kristensen, and S. Ramachandran**, Soliton self-mode conversion: revisiting raman scattering of ultrashort pulses. Optica, 6(3):304–308, 2019.
11. **K. Krupa, A. Tonello, A. Barthélémy, et al.**, Observation of geometric parametric instability induced by the periodic spatial self-imaging of multimode waves. Phys. Rev. Lett., 116:183901, May 2016.
12. **L. G Wright, D. N Christodoulides, and F. W. Wise**, Spatiotemporal mode-locking in multimode fiber lasers. Science, 358(6359):94–97, 2017.
13. **L. G. Wright, P. Sidorenko, H. Pourbeyram, et al.**, Mechanisms of spatiotemporal mode-locking. Nat. Phys., 2020.
14. **K. Krupa, A. Tonello, B. M. Shalaby, et al.**, Spatial beam self-cleaning in multimode fibres. Nature Photonics, 11:237–241, 4 2017.
15. **Z. Li, J. Zhou, B. He, Q. Lou, and D. Xue**, Beam quality of multimode fiber lasers using coiling technique. Optik, 124(1):82–84, 2013.
16. **Y. Leventoux, G. Granger, K. Krupa, et al**, 3d time-domain beam mapping for studying nonlinear dynamics in multimode optical fibers. Optics Letters, 46(1):66–69, 2021.
17. **E. V Podivilov, D. S. Kharenko, V. A. Gonta, et al.**, Hydrodynamic 2d turbulence and spatial beam condensation in multimode optical fibers. Physical Review Letters, 122(10):103902, 2019.
18. **F. O. Wu, A. U. Hassan, and D. N. Christodoulides**, Thermodynamic theory of highly multimoded nonlinear optical systems. Nat. Photonics, 13(11):776–782, 2019.
19. **T. Hansson, A. Tonello, T. Mansuryan, et al.**, Nonlinear beam self-imaging and self-focusing dynamics in a grin multimode optical fiber: theory and experiments. Optics Express, 28(16):24005–24021, 2020.

20. **N. B. Terry, T. G. Alley, and T. H Russell**, An explanation of srs beam cleanup in graded-index fibers and the absence of srs beam cleanup in step-index fibers. Optics Express, 15(26):17509–17519, 2007.
21. **G. Lopez-Galmiche, Z. Sanjabi Eznaveh, M. A. Eftekhar, et al.**, Visible supercontinuum generation in a graded index multimode fiber pumped at 1064 nm. Optics Letters, 41:2553, 6 2016.
22. **B. Crosignani and P. Di Porto**, Soliton propagation in multimode optical fibers. Optics Letters, 6(7):329–330, 1981.
23. **B. Crosignani, A. Cutolo, and P. Di Porto**, Coupled-mode theory of nonlinear propagation in multimode and single-mode fibers: envelope solitons and self-confinement. JOSA, 72(9):1136–1141, 1982.
24. **Y. An, L. Huang, J. Li, et al.**, Deep Learning-Based Real-Time Mode Decomposition for Multimode Fibers. IEEE J. Sel. Top. Quantum Electron., 26(4):1–6, 2020.
25. **L. Li, J. Leng, P. Zhou, and J. Chen**, Multimode fiber modal decomposition based on hybrid genetic global optimization algorithm. Optics Express, 25(17):19680–19690, 2017.
26. **C. Schulze, D. Naidoo, D. Flamm, et al.**, Wavefront reconstruction by modal decomposition. Optics Express, 20(18):19714–19725, 2012.
27. **G. Pariente, V. Gallet, A. Borot, O. Gobert, and F. Quéré**, Space-time characterization of ultra-intense femtosecond laser beams. Nat. Photonics, 10(8):547–553, 2016.
28. **D. Flamm, D. Naidoo, C. Schulze, A. Forbes, and M. Duparré**, Mode analysis with a spatial light modulator as a correlation filter. Optics Letters, 37(13):2478–2480, 2012.
29. **D. Flamm, C. Schulze, D. Naidoo, S. Schroter, A. Forbes, and M. Duparre**, All-digital holographic tool for mode excitation and analysis in optical fibers. Journal of Lightwave Technology, 31:1023–1032, 2013.
30. **M. Geshiro, M. Matsuhara, and N. Kumagal**, Truncated parabolic-index fiber with minimum mode dispersion. IEEE Transactions on Microwave Theory and Techniques, 26:115–119, 1978.
31. **R. Olshansky**, Propagation in glass optical waveguides. Reviews of Modern Physics, 51(2):341, 1979.
32. **A. Trichili, K. H. Park, M. Zghal, B. S. Ooi, and M. S. Alouini**, Communicating using spatial mode multiplexing: Potentials, challenges, and perspectives. IEEE Communications Surveys and Tutorials, 21:3175–3203, 10 2019.
33. **J. W. Goodman**, Introductiont to Fourier Optics. 2005.
34. **T. Kaiser, D. Flamm, S. Schröter, and M. Duparré**, Complete modal decomposition for optical fibers using cgh-based correlation filters. Optics Express, 17:9347, 2009.
35. **M. D. Gervaziev, I. Zhdanov, D. S. Kharenko, et al.**, Mode decomposition of multimode optical fiber beams by phase-only spatial light modulator. Laser Phys. Lett., 18(1):015101, jan 2020.
36. **P. Aschieri, J. Garnier, C. Michel, V. Doya, and A. Picozzi**, Condensation and thermalization of classsical optical waves in a waveguide. Physical Review A, 83(3):033838, 2011.
37. **E. V. Podivilov, F. Mangini, O. S. Sidelnikov, M. Ferraro, M. Gervaziev, D. S. Kharenko, M. Zitelli, M. P. Fedoruk, S. A. Babin, and S. Wabnitz**, Thermalization of orbital angular momentum beams in multimode optical fibers. Physical Review Letters, 128(24):243901, 2022.
38. **M. Ferraro, F. Mangini, M. Zitelli, A. Tonello, A. De Luca, V. Courderc, and S. Wabnitz**, Femtosecond nonlinear losses in multimode optical fibers. Photonics Research, 9(12), 2021.

39. **A. Mafi**. Pulse propagation in a short nonlinear graded-index multimode optical fiber. Journal of Lightwave Technology, 30(17):2803–2811, 2012.
40. **F. Mangini, M. Gervaziev, M. Ferraro, D. S. Kharenko, M. Zitelli, Y. Sun, V. Couderc, E. V. Podivilov, S. A. Babin, and S. Wabnitz**, Statistical mechanics of beam self-cleaning in grin multimode optical fibers. Optics Express, 30(7):10850–10865, 2022.
41. **K. Baudin, A. Fusaro, K. Krupa, J. Garnier, S. Rica, G. Millot, and A. Picozzi**, Classical Rayleigh-Jeans condensation of light waves: Observation and thermodynamic characterization. Physical Review Letters, 125(24):244101, 2020.
42. **H. Pourbeyram, P. Sidorenko, F. O. Wu, et al.**, Direct observations of thermalization to a rayleigh–jeans distribution in multimode optical fibres. Nature Physics, pages 1–6, 2022.
43. **F. Mangini, M. Ferraro, M. Zitelli, et al.**, Rainbow archimedean spiral emission from optical fibres. Scientific Reports, 11(13030):1–10, 2021.
44. **F. Mangini, M. Ferraro, M. Zitelli, et al**, Helical plasma filaments from the self-channeling of intense femtosecond laser pulses in optical fibers. Optics Letters, 47(1):1–4, 2022.
45. **Ya. Glick, V. Fromzel, J. Zhang, N. Ter-Gabrielyan, and M. Dubinskii**, High-efficiency, 154 W CW, diode-pumped Raman fiber laser with brightness enhancement. Appl. Opt., 56(3):B97, jan 2017.
46. **E. A. Zlobina, S. I. Kablukov, A. A. Wolf, A. V. Dostovalov, and S. A. Babin**, Nearly single-mode Raman lasing at 954 nm in a graded-index fiber directly pumped by a multimode laser diode. Opt. Lett., 42(1):9, 2017.
47. **A. G. Kuznetsov, S. I. Kablukov, A. A. Wolf, I. N. Nemov, V. A. Tyrtyshnyy, D. V. Myasnikov, and S. A. Babin**, 976 nm all-fiber raman laser with high beam quality at multimode laser diode pumping. Laser Phys. Lett., 16(10), 2019.
48. **A. G. Kuznetsov, S. I. Kablukov, E. V. Podivilov, and S. A. Babin**, Brightness enhancement and beam profiles in an LD-pumped graded-index fiber Raman laser. OSA Contin., 4(3):1034, 2021.
49. **D. S. Kharenko, M. D. Gervaziev, A. G. Kuznetsov, et al.**, Mode-resolved analysis of pump and stokes beams in ld-pumped grin fiber raman lasers. Optics Letters, 47(5):1222–1225, 2022.
50. **S. A. Babin, A. G. Kuznetsov, O. S. Sidelnikov, et al.**, Spatio-spectral beam control in multimode diode-pumped Raman fibre lasers via intracavity filtering and Kerr cleaning. Sci. Rep., 11(1):21994, dec 2021.

Received 31.10.2022
Revised 02.12.2022
Accepted 02.12.2022